International Journal of Heat and Mass Transfer 65 (2013) 765–778

Contents lists available at SciVerse ScienceDirect

International Journal of Heat and Mass Transfer

journal homepage: www.elsevier.com/locate/ijhmt

The effect of conducting boundaries on Lapwood–Prats convection

D. Andrew S. Rees [a,*], A. Mojtabi [b]

[a] Department of Mechanical Engineering, University of Bath, Bath BA2 7AY, UK
[b] Université de Toulouse, INPT, UPS, IMFT (Institut de Mécanique des Fluides de Toulouse), Allé Camille Soula, F-31400 Toulouse, France

ARTICLE INFO

Article history:
Received 29 December 2012
Accepted 31 May 2013

Keywords:
Porous medium
Horizontal throughflow
Conducting boundaries
Linear theory

ABSTRACT

We investigate the onset of convection in a uniform, constant-thickness, horizontal porous layer which is heated from below. The layer is bounded above and below by thermally conducting but impermeable layers. Our aim is to determine the effect on the onset of convection of the interaction between the presence of these outer conducting layers and a horizontal background flow. A linear stability analysis is performed and a dispersion relation is derived from which the stability characteristics of the layer are computed. Convection cells are found move along the layer at a speed which is lower than that of the imposed flow due to a thermal drag caused by the presence of the bounding solid layers. Neutral curves and streamline/isotherm patterns are presented in order to understand the physical role played by the governing nondimensional parameters. When the diffusivity of the solid layers is much lower than the diffusivity of the porous layer there exists a regime where the neutral curve can exhibit two minima, and at one point in parameter space there exists a neutral curve with a quartic minimum.

1. Introduction

Convection in a horizontal porous layer heated from below continues to be a source of research attention. Whilst there is undoubtedly a widespread range of practical topics for which heat and mass transfer in porous layers provide a good model, convective flows nevertheless are source of fundamental interest from the points of view of phenomenology (such as pattern selection) and the application of the latest analytical and numerical methods.

Horton and Rogers [1] and Lapwood [2] were the first to study the onset of convection for what may be termed the classical Darcy– Bénard problem, namely that of a uniform, isotropic horizontal porous layer which is saturated by a Newtonian fluid, and which is subject to a uniformly hot lower bounding surface and a uniformly cold upper surface. Convection arises in an infinitely long layer when the Darcy–Rayleigh number exceeds $4\pi^2$. The first mode to appear has the wavenumber, π, which corresponds to convection rolls with a square cross-section. Weakly nonlinear theory, which applies when the flow is just supercritical, shows that two-dimensional rolls form the stable planform for convection, as opposed to hexagonal cells, square or rectangular cells, or more exotic shapes – see Rees and Riley [3,4] and Rees [5]. When the bounding surfaces are heated by means of a constant heat flux, then the critical Darcy–Rayleigh number is reduced to 12 and the critical wavenumber is zero (Nield [6]). Recent weakly nonlinear studies by Rees and Mojtabi [7] suggest that the the postcritical stable planform of this constant-heat-flux form of the Darcy–Bénard problem is three dimensional. More detail may be found in the chapters by Rees [8], Tyvand [9], Rees et al. [10] and Nguyen-Quang et al. [11], and the books by Pop and Ingham [12] and Nield and Bejan [13].

In the present paper we will study one particular type of layered system. Layering arises naturally in the real world and an early paper by Rana et al. [14] was aimed at describing convection in the Pahoa reservoir in Hawaii, a system which was modelled using three porous sublayers. This numerical study displayed how the familar two dimensional convection patterns for the single-layer problem are modified substantially when layering is present. A more comprehensive approach was undertaken by McKibbin and O'Sullivan [15], who determined the conditions for the onset of convection in both two- and three-sublayer configurations. The extra degree of freedom which arises when a porous layer consists of as few as two sublayers means that the neutral curve can exhibit more unusual shapes than the standard one where one minimum is present. There is a regime in parameter space where two minima are possible; typically one of these corresponds to a local convection pattern (i.e. mainly confined to the sublayer with the higher permeability - the higher wavenumber case) or to a global pattern (the lower wavenumber). Rees and Riley [16] also presented a three-layer case where modes with three different wavenumbers become unstable at the same Darcy–Rayleigh number.

Of more specific interest to us here are the three-layer configurations where the outer layers are impermeable heat-conducting solids. If the outer layers are relatively thin, then such a configuration may be used to model experimental studies where a saturated porous medium must be bounded by some impermeable barrier;

* Corresponding author. Tel.: +44 1225 386775.
E-mail address: D.A.S.Rees@bath.ac.uk (D. Andrew S. Rees).

0017-9310/$ - see front matter © 2013 Elsevier Ltd. All rights reserved.
http://dx.doi.org/10.1016/j.ijheatmasstransfer.2013.05.071

Nomenclature

A,B,C,D,E	constants
c	phase velocity
d	conductivity ratio
g	gravity
k	disturbance wavenumber
k	thermal conductivity
K	permeability
p	pressure
Pe	Péclet number
Ra	Darcy–Rayleigh number
t	time
u	horizontal velocity
w	vertical velocity
x	horizontal coordinate
z	vertical coordinate

Greek symbols

α	diffusivity ratio
β	thermal expansion coefficient
γ	constant
Γ	exponent
δ	thickness ratio
θ	fluid temperature
Θ	disturbance fluid temperature
κ	thermal diffusivity
λ,σ	exponential growth rate
μ	dynamic viscosity
ρ	density
ψ	streamfunction
Ψ	disturbance streamfunction

Subscripts and superscripts

1,2,3	sublayer
c	critical value
ref	reference value
$'$	derivative with respect to z
$\wedge$	dimensional

see Rees and Mojtabi [7] and Mojtabi and Rees [17]. An early paper by Riahi [18] considered infinitely thick solid sublayers and he used weakly nonlinear theory to show that the convection planform may, when the conductivity of the solid layers is small, take the form of three-dimensional cells with a square planform. His analysis was extended to solid layers of finite thickness by Rees and Mojtabi [7].

A different, but practically important, modification of the classical Darcy–Bénard problem was undertaken by Prats [19] who considered the effect of a horizontal pressure gradient. When Darcy's law applies, this pressure gradient induces a uniform fluid velocity along the layer, unlike the parabolic velocity profile which arises in plane-Poiseuille flow. Prats showed that the convection cells found by Horton and Rogers [1] and Lapwood [2] move along the layer with exactly the velocity of the background flow. A simple coordinate transformation to a frame of reference which moves with the background flow removes the background velocity from the governing equations, even when under strongly supercritical conditions. Thus the vertical heat transfer and all the nonlinear dynamics are unaffected by this forced convection component.

The aim of the present work, then, is to determine how the presence of conducting boundaries affects the simple result of Prats [19], namely, that the phase velocity of the convection cells is precisely the same as the velocity of the background flow. It is a simple piece of *a priori* reasoning that the presence of stationary bounding surfaces will impose a thermal drag on the cells, and therefore the velocity of the cells should lie between zero and that of the background flow. But the present paper also addresses the question of whether this three-layer system displays any unusual behaviour over and above having a simple minimum in the neutral curve.

The linear stability analysis which we present is facilitated by the derivation of a dispersion relation which takes the form of a complex 4×4 determinant. Setting the real and imaginary parts to zero simultaneously yields both the critical Darcy–Rayleigh number and the phase velocity of the cells. We present neutral curves and the variation of the critical values of the Darcy–Rayleigh number, wavenumber and phase velocity as a function of the diffusivity ratio, conductivity ratio, thickness ratio and the Péclet number. The behaviour of these curves is explained by means of a selection of streamline/isotherm plots. We find that the classical unimodal neutral curve does indeed occasionally take a more exotic form, and this corresponds to when the diffusivity of the solid layers is substantially less than that of the porous layer.

2. Governing equations

We investigate the effect of conducting boundaries on what we shall call the Lapwood-Prats problem, namely the Darcy–Bénard problem modified by the presence of a horizontal forced convective pressure gradient. The detailed configuration we consider is shown in Fig. 1 and it is comprised of a uniform isotropic saturated porous layer of thickness, h_2, which is bounded by two uniform, impermeable but thermally conducting plates with thicknesses, h_1 and h_3. These plates do not necessarily have identical conductivities or thicknesses and the derivation of our stability analysis will maintain this, but we will present detailed results only for those cases where the solid layers are identical in every respect. This three-sublayer composite system is taken to be of infinite extent in both horizontal directions.

The origin of the coordinate system is located at the bottom of the composite layer, while $\hat{x}$ and $\hat{z}$ are the horizontal vertical coordinates, respectively. Constant but different temperatures are imposed at the external surfaces of the composite layer, i.e. at $\hat{z} = 0$ and at $\hat{z} = h_1 + h_2 + h_3$, where the lower surface is hotter than the upper surface. The somewhat unusual formula given in Fig. 1 for the temperature of the upper surface means that the overall temperature difference across the porous layer is ΔT. The Darcy–Rayleigh number will be defined using this value, this allows our results to be compared easily with single-layer systems, or systems where the solid layers are exceptionally thick.

For convenience the sublayers are numbered, 1, 2 and 3, beginning with the lowest sublayer. We will assume that the ensuing convection is restricted to being two-dimensional and therefore the full governing equations for the porous layer are,

$$\frac{\partial \hat{u}}{\partial \hat{x}} + \frac{\partial \hat{w}}{\partial \hat{z}} = 0, \tag{1}$$

$$\hat{u} = -\frac{K}{\mu}\frac{\partial \hat{p}}{\partial \hat{x}}, \quad \hat{w} = -\frac{K}{\mu}\frac{\partial \hat{p}}{\partial \hat{z}} + \frac{\rho_2 g \beta K}{\mu}(T_2 - T_{\mathrm{ref}}), \tag{2}$$

$$(\rho C)_2 \frac{\partial T_2}{\partial t} + (\rho C)_f \left(\hat{u}\frac{\partial T_2}{\partial \hat{x}} + \hat{w}\frac{\partial T_2}{\partial \hat{z}} \right) = k_2 \left(\frac{\partial^2 T_2}{\partial \hat{x}^2} + \frac{\partial^2 T_2}{\partial \hat{z}^2} \right), \tag{3}$$

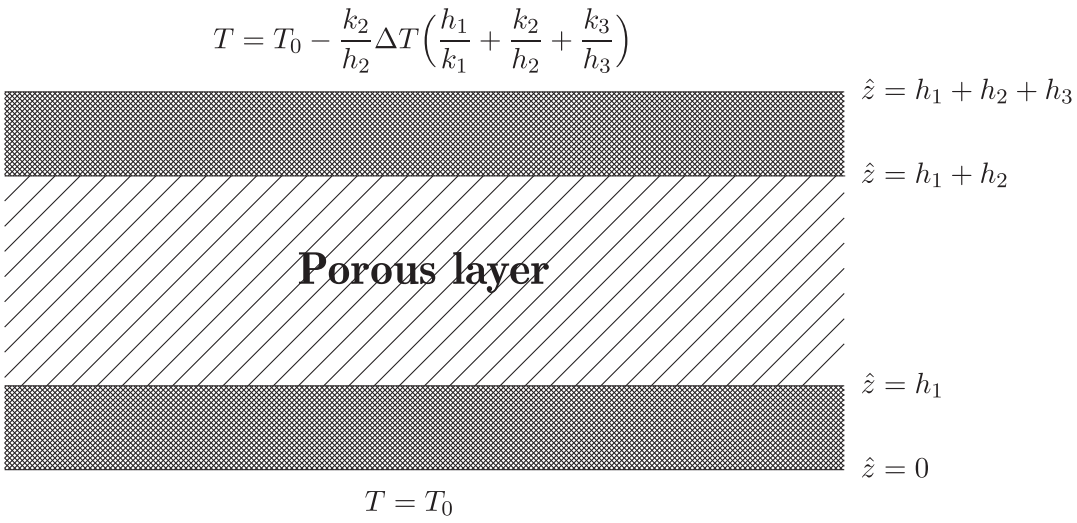

Fig. 1. Definition sketch of the configuration being studied. The porous layer is sandwiched between two impermeable but thermally conducting layers. The value, ΔT, is the temperature drop across the porous layer.

where all quantities are given in the Nomenclature. The respective equations for conductive heat transfer in the solid sublayers are,

$$(\rho C)_1 \frac{\partial T_1}{\partial \hat{t}} = k_1\left(\frac{\partial^2 T_1}{\partial \hat{x}^2} + \frac{\partial^2 T_1}{\partial \hat{z}^2}\right) \tag{4}$$

and

$$(\rho C)_3 \frac{\partial T_3}{\partial \hat{t}} = k_3\left(\frac{\partial^2 T_3}{\partial \hat{x}^2} + \frac{\partial^2 T_3}{\partial \hat{z}^2}\right). \tag{5}$$

The boundary and interface conditions are,

$$\begin{aligned}
&\hat{z} = 0: \quad T_1 = T_{\mathrm{ref}},\\
&\hat{z} = h_1: \quad \hat{w} = 0, \quad T_1 = T_2, \quad k_1\frac{\partial T_1}{\partial \hat{z}} = k_2\frac{\partial T_2}{\partial \hat{z}},\\
&\hat{z} = h_1 + h_2: \quad \hat{w} = 0, \quad T_2 = T_3, \quad k_2\frac{\partial T_2}{\partial \hat{z}} = k_3\frac{\partial T_3}{\partial \hat{z}},\\
&\hat{z} = h_1 + h_2 + h_3: \quad T_3 = -\frac{k_2}{h_2}\Delta T\left(\frac{h_1}{k_1} + \frac{h_2}{k_2} + \frac{h_3}{k_3}\right) + T_{\mathrm{ref}}.
\end{aligned} \tag{6}$$

The imposed horizontal pressure gradient is of such a magnitude that it induces the velocity field, $(u,v) = (U,0)$.

The following scalings may be introduced in order to render nondimensional the governing equations:

$$\begin{aligned}
&\hat{x} = h_2 x, \quad \hat{z} = h_1 + h_2 z, \quad \hat{t} = \frac{h_2^2(\rho C)_2}{k_2}t, \quad \hat{p} = \frac{k_2\mu}{(\rho C)_f K}p,\\
&(\hat{u}, \hat{v}, \hat{w}) = \frac{k_2}{h_2(\rho C)_f}(u, v, w), \quad T = T_{\mathrm{ref}} - \frac{k_2}{k_1}\frac{h_1}{h_2}\Delta T + \Delta T\ \theta,
\end{aligned} \tag{7}$$

which are based on the height and the properties of the porous layer.

We thereby obtain the nondimensional equations:

$$\frac{\partial u}{\partial x} + \frac{\partial w}{\partial z} = 0, \tag{8}$$

$$u = -\frac{\partial p}{\partial x}, \quad w = -\frac{\partial p}{\partial z} + \mathrm{Ra}\,\theta_2, \tag{9}$$

$$\frac{\partial \theta_2}{\partial t} + u\frac{\partial \theta_2}{\partial x} + w\frac{\partial \theta_2}{\partial z} = \frac{\partial^2 \theta_2}{\partial x^2} + \frac{\partial^2 \theta_2}{\partial z^2}, \tag{10}$$

$$\frac{\partial \theta_1}{\partial t} = \alpha_1\left(\frac{\partial^2 \theta_1}{\partial x^2} + \frac{\partial^2 \theta_1}{\partial z^2}\right) \tag{11}$$

and

$$\frac{\partial \theta_3}{\partial t} = \alpha_3\left(\frac{\partial^2 \theta_3}{\partial x^2} + \frac{\partial^2 \theta_3}{\partial z^2}\right). \tag{12}$$

The diffusivity ratios, α_1 and α_3, are defined according to,

$$\alpha_1 = \frac{k_1(\rho C)_2}{k_2(\rho C)_1}, \quad \alpha_3 = \frac{k_3(\rho C)_2}{k_2(\rho C)_3}. \tag{13}$$

The Darcy–Rayleigh number is defined to be,

$$\mathrm{Ra} = \frac{\rho_2(\rho C)_f g\beta h_2 K\Delta T}{\mu k_2} \tag{14}$$

and it is based upon the height of the porous layer and the temperature difference across it. The two conductivity and thickness ratios as follows,

$$d_1 = k_1/k_2, \quad d_3 = k_3/k_2, \quad \delta_1 = h_1/h_2, \quad \delta_3 = h_3/h_2. \tag{15}$$

The background velocity is now $(u,w) = (0,\mathrm{Pe})$, where the Péclet number is given by,

$$\mathrm{Pe} = \frac{h_2 U}{k_2(\rho C)_f}. \tag{16}$$

For two-dimensional flow we may define the streamfunction, ψ, using,

$$u = -\frac{\partial \psi}{\partial z} \quad \text{and} \quad w = \frac{\partial \psi}{\partial x} \tag{17}$$

and the full governing equations become

$$\frac{\partial^2 \psi}{\partial x^2} + \frac{\partial^2 \psi}{\partial z^2} = \mathrm{Ra}\ \frac{\partial \theta}{\partial x}, \tag{18}$$

$$\frac{\partial \theta_2}{\partial t} + \frac{\partial \psi}{\partial x}\frac{\partial \theta_2}{\partial z} - \frac{\partial \psi}{\partial z}\frac{\partial \theta_2}{\partial x} = \frac{\partial^2 \theta_2}{\partial x^2} + \frac{\partial^2 \theta_2}{\partial z^2}, \tag{19}$$

in the porous layer, and

$$\frac{\partial \theta_1}{\partial t} = \alpha_1\left(\frac{\partial^2 \theta_1}{\partial x^2} + \frac{\partial^2 \theta_1}{\partial z^2}\right), \quad \text{and} \quad \frac{\partial \theta_3}{\partial t} = \alpha_3\left(\frac{\partial^2 \theta_3}{\partial x^2} + \frac{\partial^2 \theta_3}{\partial z^2}\right), \tag{20}$$

in the bounding sublayers. The boundary and interface conditions are

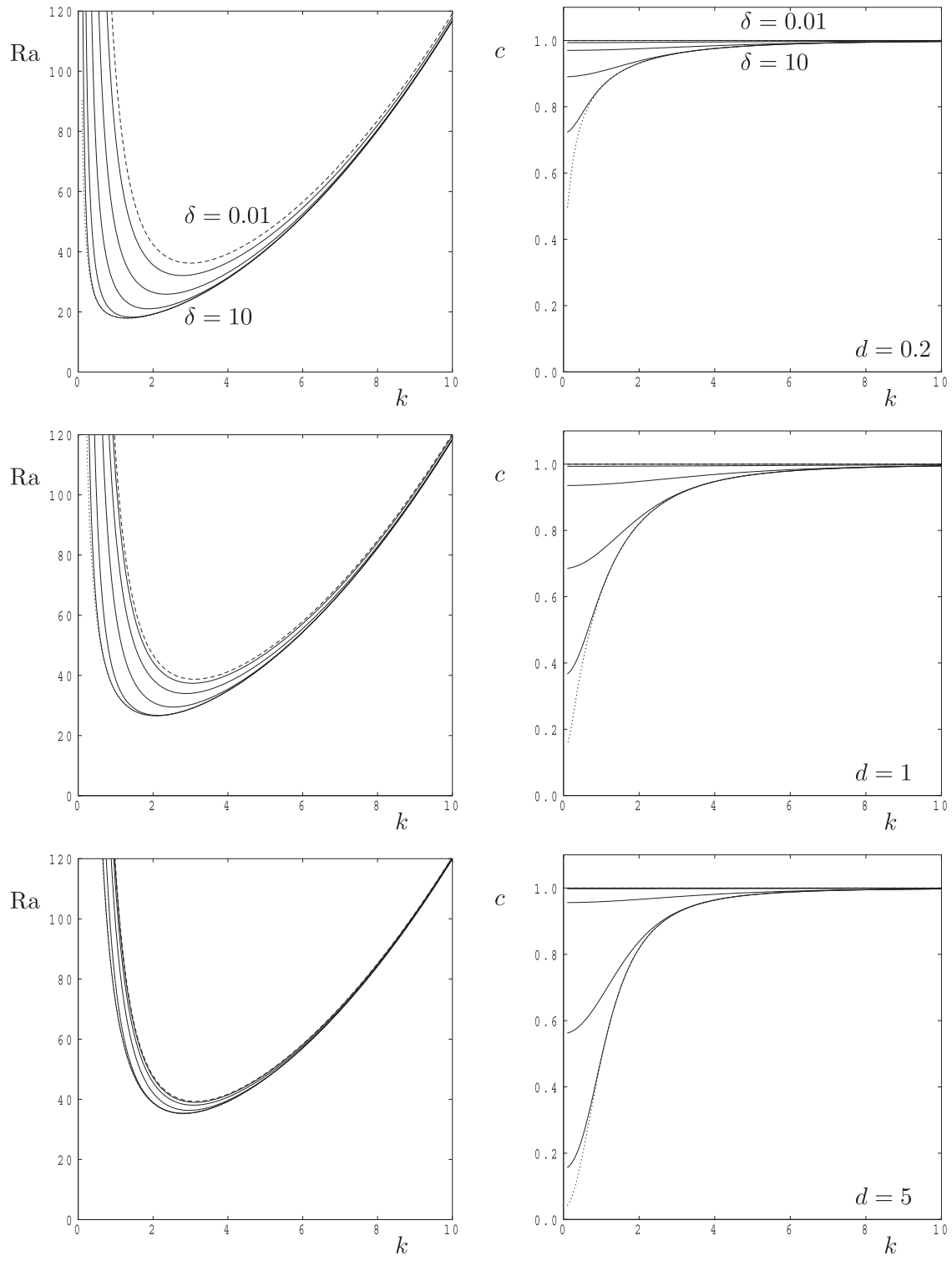

Fig. 2. Neutral curves (left) and the corresponding values of the wavespeed, c, (right) for $\alpha = 1$ and $\mathrm{Pe} = 1$ for the stated values of d. The following values of δ were used: $\delta = 10,3,1,0.3,0.1,0.03$ and 0.01. The dotted line corresponds to $\delta = 10$ and the dashed line to $\delta = 0.01$.

$$
\begin{aligned}
&z = -\delta_1: \quad \theta_1 = \delta_1/d_1,\\
&z = 0: \quad \psi = 0, \quad \theta_2 = \theta_1, \quad \frac{\partial\theta_2}{\partial z} = d_1\frac{\partial\theta_1}{\partial z},\\
&z = 1: \quad \psi = 0, \quad \theta_2 = \theta_3, \quad \frac{\partial\theta_2}{\partial z} = d_3\frac{\partial\theta_3}{\partial z},\\
&z = 1+\delta_3: \quad \theta_3 = -1 - \delta_3/d_3.
\end{aligned}
\tag{21}
$$

3. Linear stability equations

We perturb about the basic state by setting,

$$
\begin{pmatrix}\psi\\ \theta_1\\ \theta_2\\ \theta_3\end{pmatrix} = \begin{pmatrix}-\mathrm{Pe}\, z\\ 1-(z/d_1)\\ 1-z\\ (1-z)/d_3\end{pmatrix} + e^{ik(x-ct)}\begin{pmatrix}-i\Psi(z)\\ \Theta_1(z)\\ \Theta_2(z)\\ \Theta_3(z)\end{pmatrix} + \text{c.c.}, \tag{22}
$$

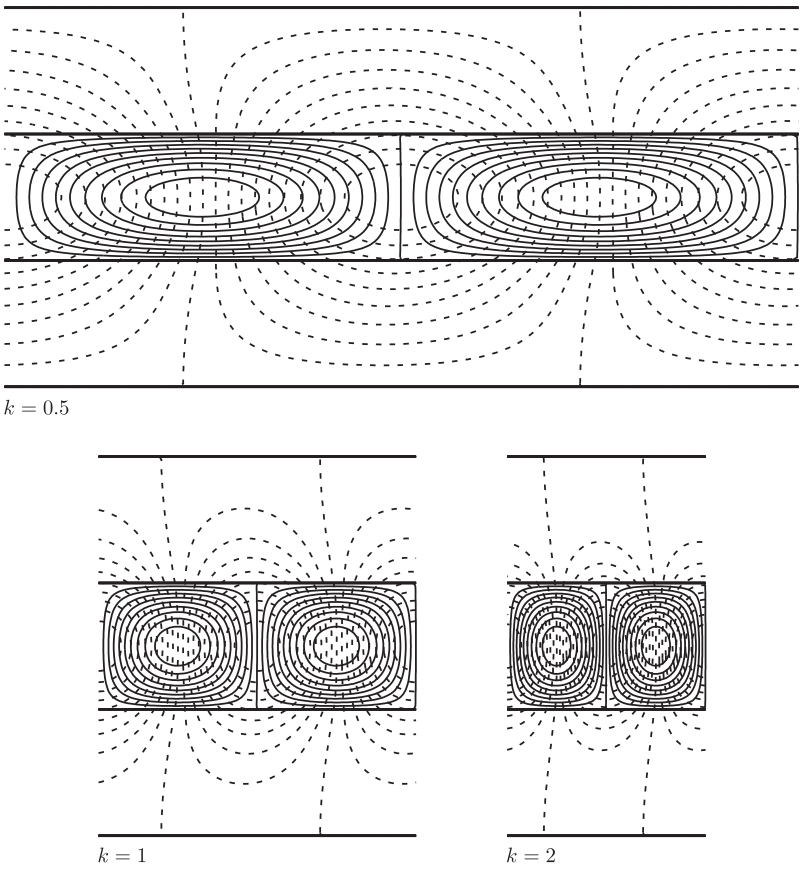

Fig. 3. Streamlines (continuous lines) and isotherms (dashed lines) for $d = \delta = \alpha = \mathrm{Pe} = 1$. Showing the effect of having different wavenumbers.

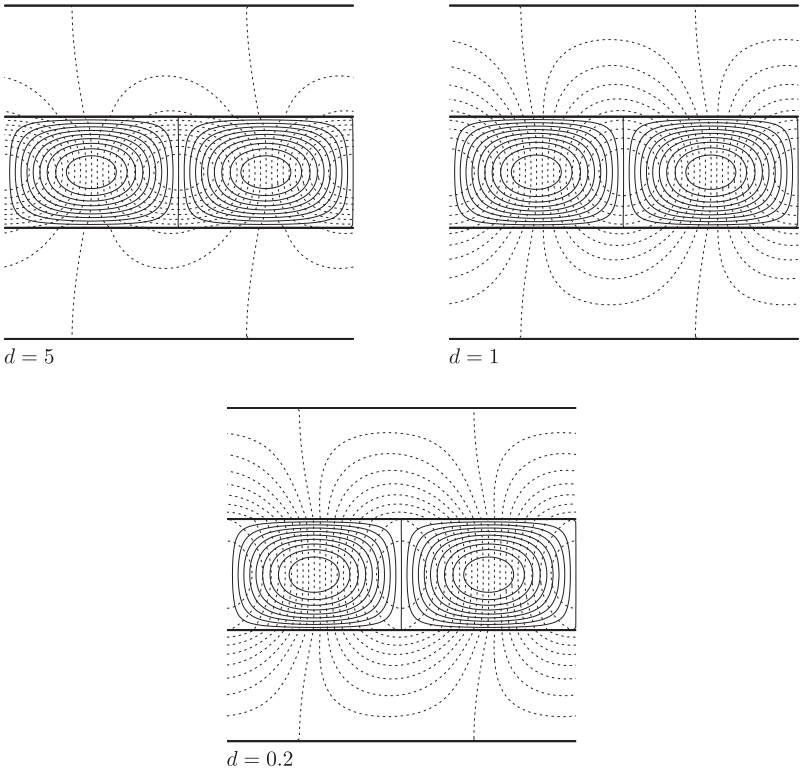

Fig. 4. Streamlines (continuous lines) and isotherms (dashed lines) for $\delta = \alpha = \mathrm{Pe} = 1$. The wavenumber is $k = 1$. Showing the effect of having different conductivity ratios.

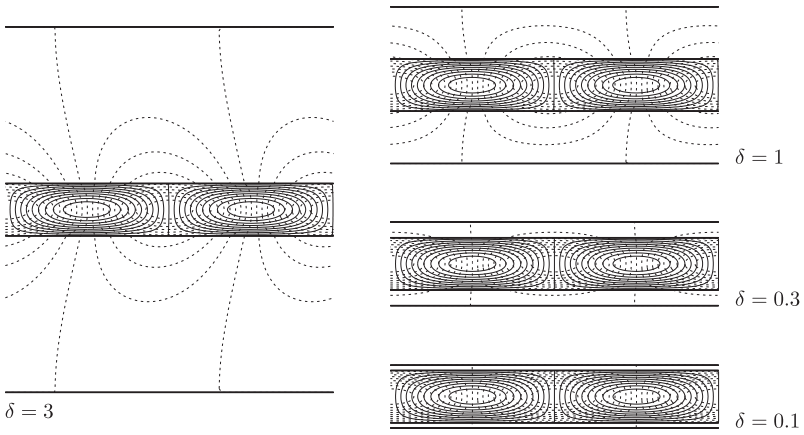

Fig. 5. Streamlines (continuous lines) and isotherms (dashed lines) for α = Pe = 1 and d = 5. The wavenumber is k = 1. Showing the effect of having different values of δ.

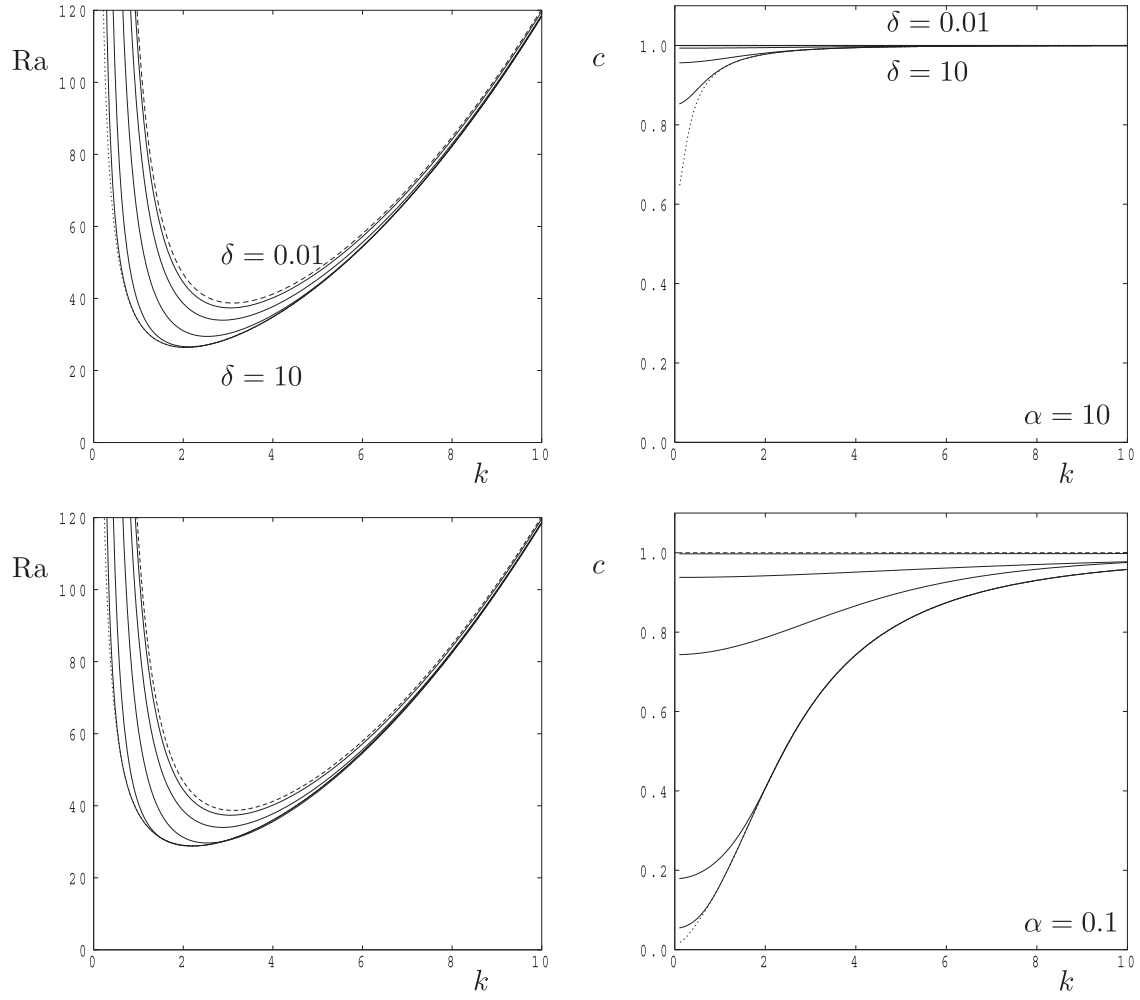

Fig. 6. Neutral curves (left) and the corresponding values of the wavespeed, c, (right) for d = 1 and Pe = 1 for the stated values of α. The following values of δ were used: δ = 10,3,1,0.3,0.1,0.03 and 0.01. The dotted line corresponds to δ = 10 and the dashed line to δ = 0.01.

where k is the wavenumber and c is the phase velocity of the cell pattern. The linearized stability equations now take the ordinary differential form,

$$\Psi'' - k^2\Psi + \mathrm{Ra}\ k\Theta_2 = 0, \tag{23}$$

$$\Theta_1'' - (k^2 - ikc/\alpha_1)\Theta_1 = 0, \tag{24}$$

$$\Theta_2'' - (k^2 + ik(\mathrm{Pe} - c))\Theta_2 + k\Psi = 0, \tag{25}$$

$$\Theta_3'' - (k^2 - ikc/\alpha_3)\Theta_3 = 0, \tag{26}$$

where the boundary conditions are:

$$\begin{aligned} z = -\delta_1: &\quad \Theta_1 = 0, \\ z = 0: &\quad \Psi = 0, \quad \Theta_2 = \Theta_1, \quad \Theta_2' = d_1\Theta_1', \\ z = 1: &\quad \Psi = 0, \quad \Theta_2 = \Theta_3, \quad \Theta_2' = d_3\Theta_3', \\ z = 1 + \delta_3: &\quad \Theta_3 = 0. \end{aligned} \tag{27}$$

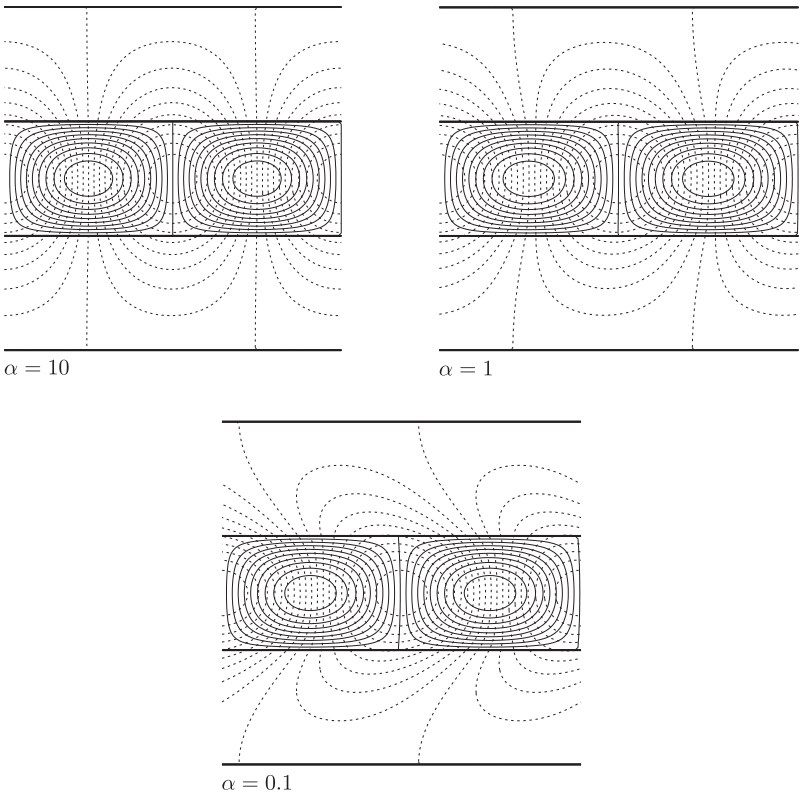

Fig. 7. Streamlines (continuous lines) and isotherms (dashed lines) for $\delta = d = \mathrm{Pe} = 1$. The wavenumber is $k = 2$. Showing the effect of having different diffusivity ratios, α.

4. The dispersion relation

In layer 1 the solution which satisfies the boundary condition at $z = -\delta_1$ is

$$\Theta_1 = A \sinh \lambda_1 (z + \delta_1), \tag{28}$$

where

$$\lambda_1 = \left(k^2 - i \frac{kc}{\alpha_1} \right)^{1/2} \tag{29}$$

and hence $\Theta_1' = A\lambda_1 \cosh \lambda_1 (z + \delta_1)$. If we now apply the $z = 0$ interface conditions which are given by (27) we find that,

$$\Theta_2(0) = A \sinh \lambda_1 \delta_1, \quad \Theta_2'(0) = A\lambda_1 d_1 \cosh \lambda_1 \delta_1. \tag{30}$$

Given that the constant, A, is arbitrary, these two conditions for $\Theta_2(0)$ and $\Theta_2'(0)$ may be combined to remove A, which thereby yields the following boundary condition of the third kind,

$$\Theta_2(0) = \frac{\tanh \lambda_1 \delta_1}{\lambda_1 d_1} \Theta_2'(0). \tag{31}$$

For later convenience we rewrite Eq. (31) as $\Theta_2(0) = \gamma_1 \Theta_2'(0)$ where

$$\gamma_1 = \frac{\tanh \lambda_1 \delta_1}{\lambda_1 d_1}. \tag{32}$$

The corresponding boundary condition at $z = 1$ is

$$\Theta_2(1) = -\frac{\tanh \lambda_3 \delta_3}{\lambda_3 d_3} \Theta_2'(1), \tag{33}$$

or, in compact form, as $\Theta_2(1) = -\gamma_3 \Theta_2'(1)$ where

$$\gamma_3 = \frac{\tanh \lambda_3 \delta_3}{\lambda_3 d_3} \quad \text{and} \quad \lambda_3 = \left(k^2 - i \frac{kc}{\alpha_3} \right)^{1/2}. \tag{34}$$

Therefore we are in a position to consider only the solutions within the porous layer (Eqs. (23) and (25)) where the full dynamic thermal of a mode with wavenumber k in the outer bounding layers is modelled completely by the complex boundary conditions, Eqs. (31) and (33).

Solutions of Eqs. (23) and (25) take the form, $\exp(\Gamma z)$, where Γ satisfies the determinantal equation,

$$\begin{vmatrix} \Gamma^2 - k^2 & \mathrm{Ra}\, k \\ k & \Gamma^2 - k^2 + ik(c - \mathrm{Pe}) \end{vmatrix} = 0. \tag{35}$$

Hence $\Gamma = \pm\lambda, \pm\sigma$, where

$$\lambda^2 = k^2 + ik(\mathrm{Pe} - c)/2 + k[\mathrm{Ra} - (\mathrm{Pe} - c)^2/4]^{1/2}, \tag{36}$$

$$\sigma^2 = k^2 + ik(\mathrm{Pe} - c)/2 - k[\mathrm{Ra} - (\mathrm{Pe} - c)^2/4]^{1/2}. \tag{37}$$

If we now set

$$\Psi = -\mathrm{Ra}\, k \left[\frac{A \sinh \lambda z + B \cosh \lambda z}{\lambda^2 - k^2} + \frac{C \sinh \sigma z + D \cosh \sigma z}{\sigma^2 - k^2} \right], \tag{38}$$

then

$$\Theta_2 = A \sinh \lambda z + B \cosh \lambda z + C \sinh \sigma z + D \cosh \sigma z. \tag{39}$$

Application of $\Psi(0) = 0$ leads to

$$\frac{B}{\lambda^2 - k^2} + \frac{D}{\sigma^2 - k^2} = 0, \tag{40}$$

while the condition, $\Psi(1) = 0$, gives,

$$\frac{A \sinh \lambda + B \cosh \lambda}{\lambda^2 - k^2} + \frac{C \sinh \sigma + D \cosh \sigma}{\sigma^2 - k^2} = 0. \tag{41}$$

The application of the boundary condition, Eq. (31) at $z = 0$ gives,

$$B + D = \gamma_1 (\lambda A + \sigma C), \tag{42}$$

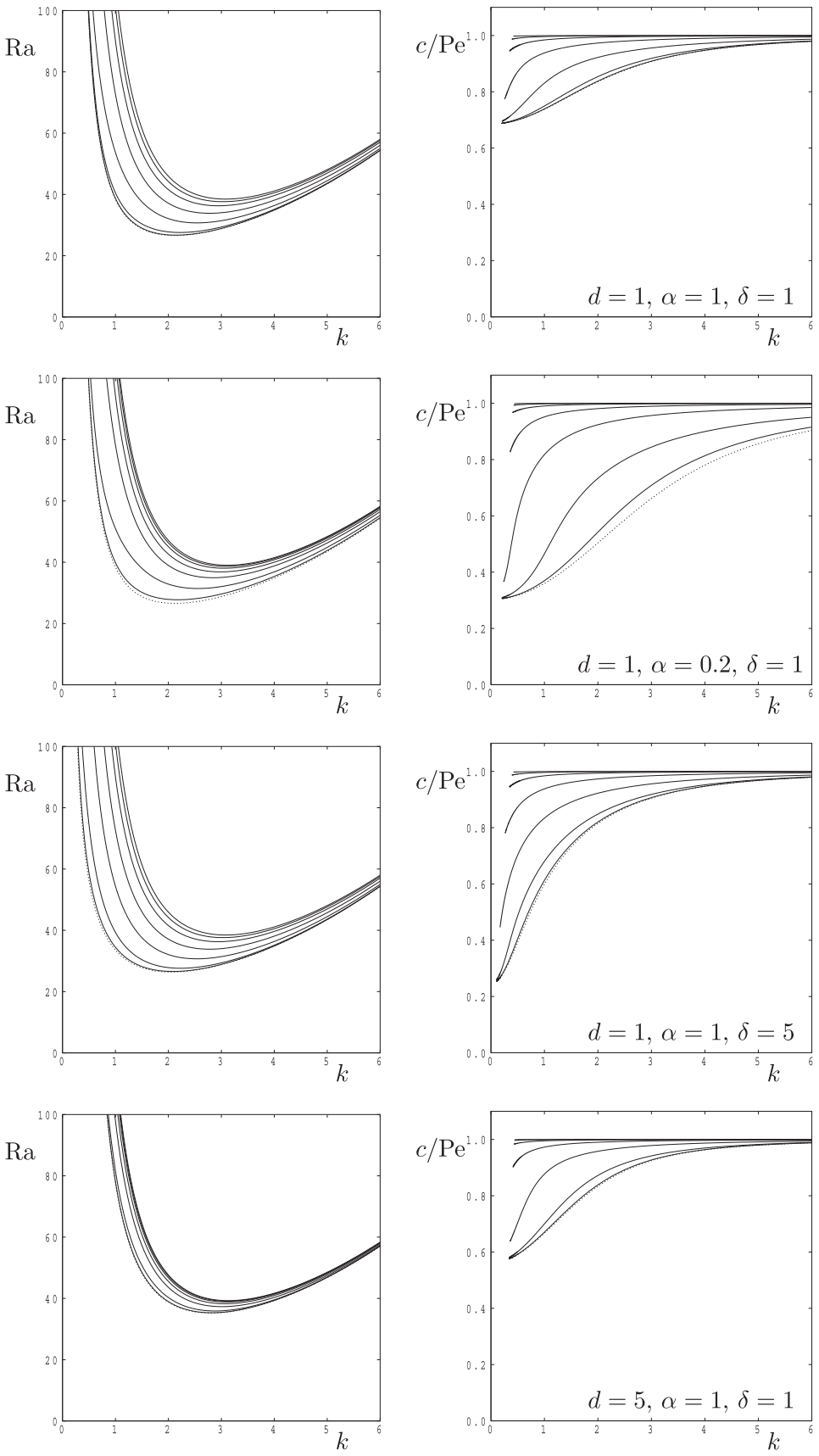

Fig. 8. Neutral curves (left) and the corresponding values of the scaled wavespeed, c/Pe, (right) $d = 1$ for the stated values of d,α and δ. The following values of Pe were used: 0,1,3,10,30,100,300 and 1000. The dotted (lowest) line corresponds to Pe = 0 and the dashed (uppermost) line to Pe = 1000.

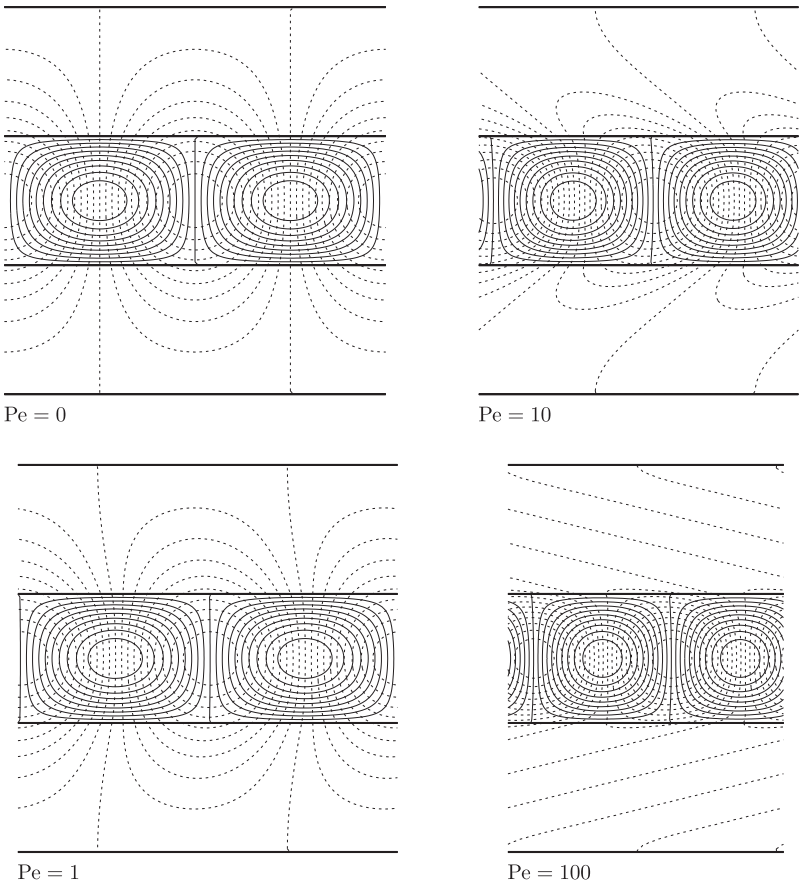

Fig. 9. Streamlines (continuous lines) and isotherms (dashed lines) for $d = \delta = \alpha = 1$. Showing the effect of having different values of the Péclet number. Each wavenumber corresponds to the minimum in the respective neutral curves.

while the boundary condition, Eq. (33), yields

$$A\sinh\lambda + B\cosh\lambda + C\sinh\sigma + D\cosh\sigma = -\gamma_3[\lambda(A\cosh\lambda + B\sinh\lambda) + \sigma(C\cosh\sigma + D\sinh\sigma)]. \quad (43)$$

These last four equations always admit zero solutions for A,B, C and D except for when Ra and c take their appropriate eigenvalues. These are found by insisting that the following complex determinant is precisely zero:

$$\begin{vmatrix} 0 & \frac{1}{\lambda^2-k^2} & 0 & \frac{1}{\sigma^2-k^2} \\ \frac{\sinh\lambda}{\lambda^2-k^2} & \frac{\cosh\lambda}{\lambda^2-k^2} & \frac{\sinh\sigma}{\sigma^2-k^2} & \frac{\cosh\sigma}{\sigma^2-k^2} \\ -\lambda\gamma_1 & 1 & -\sigma\gamma_1 & 1 \\ \sinh\lambda+\lambda\gamma_3\cosh\lambda & \cosh\lambda+\lambda\gamma_3\sinh\lambda & \sinh\sigma+\sigma\gamma_3\cosh\sigma & \cosh\sigma+\sigma\gamma_3\sinh\sigma \end{vmatrix} = 0. \quad (44)$$

This determinant generally takes complex values and therefore the setting of it to zero means that two quantities are determined as eigenvalues, namely Ra and c. This was done by means of a straightforward two-dimensional Newton–Raphson iteration scheme and the results obtained are essentially exact. Later, we present some rather unusally-shaped neutral curves which arise at an extreme value of one of the governing parameters; we therefore modified our Fortran90 code from `real*8` to `real*16` in order to check if such unusual curves arose from the accumulation of round-off error — it was found that these `real*8` results had not suffered any degradation in accuracy due to round-off error.

The locations of the minima in the neutral curves are generally found by differentiating an explicit expression for Ra with respect to k and setting this to zero. In the present problem Ra and c are given implicitly by the determinant given in (38). We therefore performed a numerical differentiation of the kind described in detail in Rees and Genç [20] to find such minima.

The full system described above is one with seven independent parameters (δ_1, δ_3, d_1, d_3, α_1, α_3 and Pe) when it is assumed that the values Ra, k and c are determined from the computation of critical values. However, we reduce the system to four parameters by insisting that the layer is symmetric, i.e. the bounding layers are identical in every way. Therefore we set $\delta_1 = \delta_3 \equiv \delta$, $d_1 = d_3 \equiv d$ and $\alpha_1 = \alpha_3 \equiv \alpha$.

5. Results and discussion

The result of our computation is presented in three different forms: neutral curves, streamline and isotherm plots and the variation of critical values. Even with four independent nondimensional parameters it is virtually impossible to give comprehensive results. Therefore we will concentrate on giving a good physical understand of the roles played by the nondimensional parameters.

We have chosen to use the case, $\delta = d = \alpha = \mathrm{Pe} = 1$, as the reference case against which most of our results will be compared.

5.1. The influence of variations in d and δ

Fig. 2 keeps the values of Pe and α fixed at 1. Neutral curves are shown for three values of d in separate graphs and for a range of values of δ in each graph. In addition to the behaviour of Ra as a function of the wavenumber, k, we also show the variation of the phase speed, c, with k.

The neutral curves show the very familiar unimodal shape with a single minimum. We note that in those cases which we have computed, including those not present in this paper, the lowest

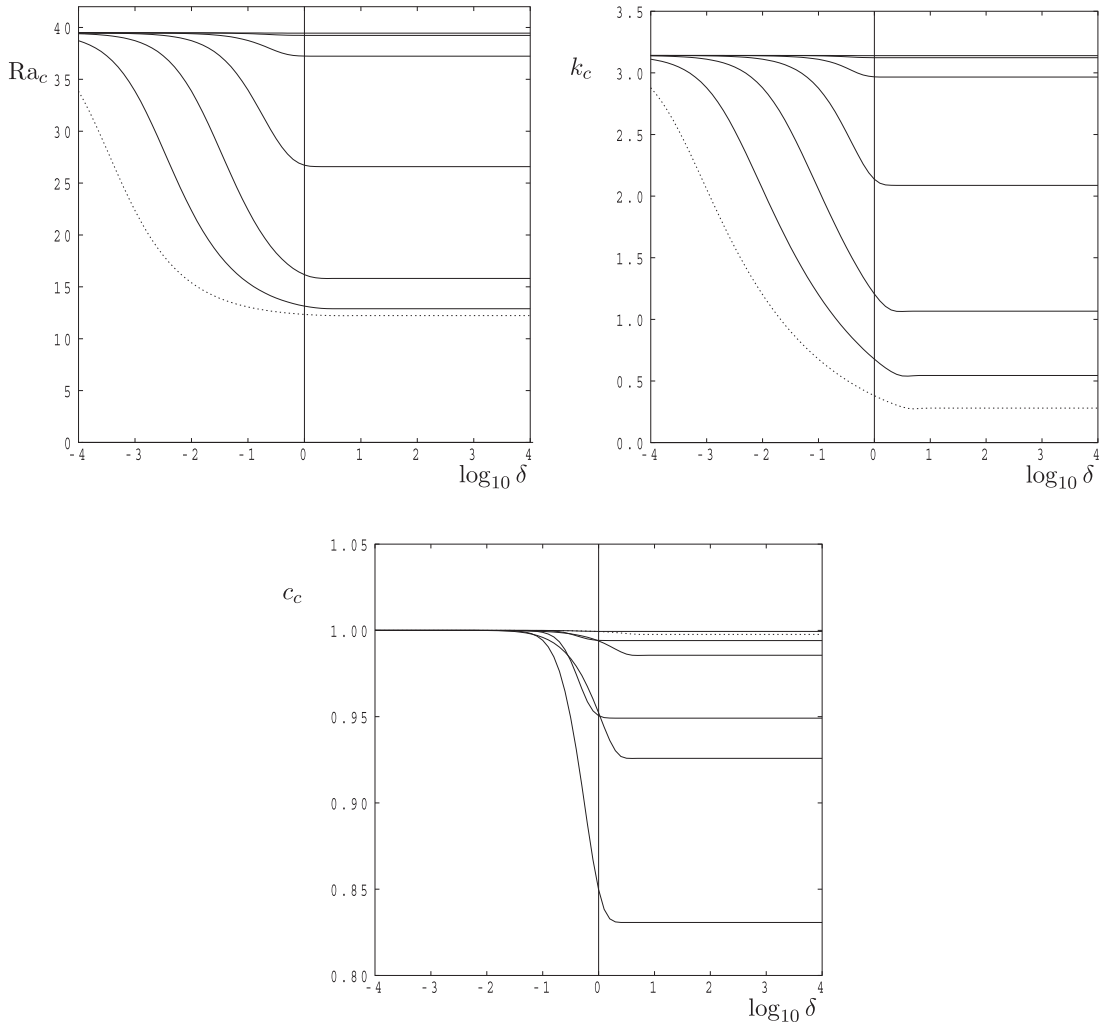

Fig. 10. Critical values for Ra,k and c as a function of δ for α = Pe = 1 and for $d = 10^{-3}$, 10^{-2},10^{-1},10^{0},10^{1},10^{2} and 10^{3}.

value of Ra always lies between 12 and $4\pi^2$. The latter arises when the solid plates are either very thin indeed ($\delta \ll 1$), which may be seen as the dashed lines here, or very highly conducting ($d \gg 1$), while the former arises when the solid plates tend towards being insulating ($d \ll 1$). These values are well-known in the context of the onset of convection in a single layer; see Nield and Bejan [13].

As the values of d and δ vary, the general behaviour of the neutral curves shown in Fig. 2, where we concentrate specifically on the critical values of the Darcy–Rayleigh number and wavenumber (Ra$_c$ and k_c, respectively), are as might be expected. For example, when $d = 0.2$, the values of Ra$_c$ and k vary greatly as the thickness of the bounding layers, δ, varies. Sufficiently thin bounding layers ($\delta = 0.01$) of low conductivity do not alter the onset criterion very much from that of the classical Darcy–Bénard problem, namely Ra$_c = 4\pi^2$ and $k_c = \pi$. On the other hand, when δ increases to large values, the lack of conductivity in the bounding layers yield an onset problem which is close to that of the classical Darcy–Bénard problem with constant heat flux boundaries. Thus the critical values are close to Ra$_c$ = 12 and $k_c = 0$ when d is small and δ is large.

It is also clear that the phase speed of the disturbances depends strongly on the wavenumber. The thermal disturbances do not penetrate far into the bounding layers when k is large, and therefore the moving cells are unaffected by the presence of the outer layers, which is why the nondimensional phase velocity is close to 1. Similarly, the bounding layers are essentially ineffective when they are thin. On the other hand, when there is a substantial penetration of the bounding layers by the thermal field, the phase velocity is affected. This is particularly true for small wavenumbers where the thermal penetration is of the same order as the wavelength of the cells.

Many of the above observations are displayed in Figs. 3–5. These Figures, and others later correspond to a snapshot of streamlines and isotherms at one point in time, the whole pattern then being understood to move to the right at the computed phase speed.

In Fig. 3 we demonstrate the changing thermal penetration as the disturbance wavenumber changes. In particular we see the penetration decreasing as k increases, and hence the disturbance phase speed increases, although here it does so by only a small amount. The phase speed is in the region of 0.9, which corresponds to the very small lag which may be seen in the isotherms in the bounding layers. Later we will see cases where the lag is greater, and this is brought about by small values of α or large values of Pe.

Similar variations in the thermal penetration into the bounding layers are seen in Fig. 4, but this is caused by having difference values of d. When d is large, the bounding layers are relatively highly conducting which causes the layers to tend towards a uniform temperature. When d is small, there is a very substantial variation in the temperature of the bounding layers. The isotherms in the porous layer when $d = 0.2$ are close to being vertical at the interfaces with the bounding layers, which is why small-d cases mimic constant heat flux single-layer convection.

The effect of variations in δ on the streamlines and isotherms are shown in Fig. 5. The case with $\delta = 3$ is quite typical of cases with

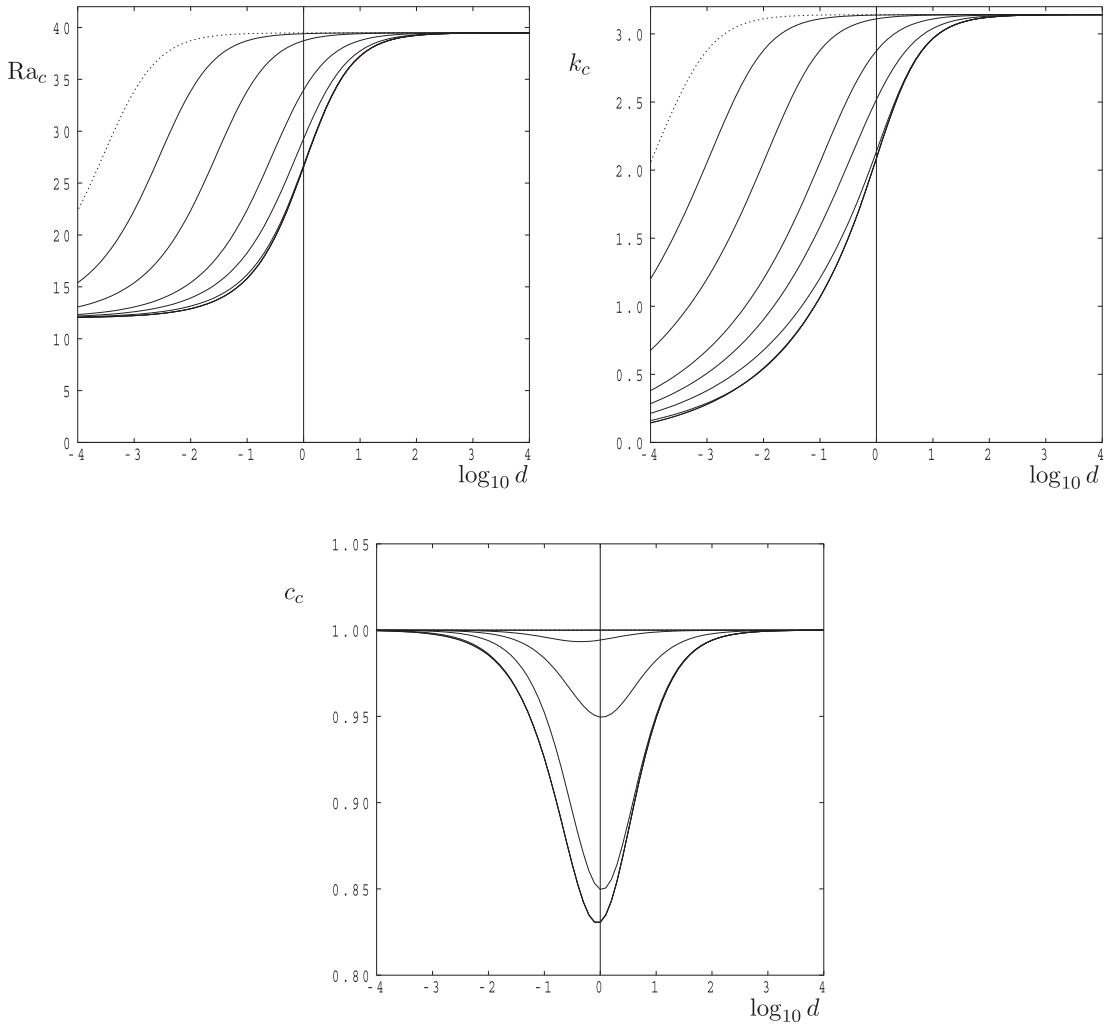

Fig. 11. Critical values for Ra,k and c as a function of d for $\alpha = \mathrm{Pe} = 1$ and for $\delta = 10^{-4}$, 10^{-3},10^{-2},10^{-1},$10^{-0.5}$,10^{0}, $10^{0.5}$,10^{1} and 10^{2}. The dotted line corresponds to $\delta = 10^{-4}$.

substantially thicker bounding layers, and the thermal disturbance is confined naturally to a region which is just thicker than the porous layer. As δ decreases to values of 1 and below, there is a decreasing amount of room for the thermal disturbance to develop within the bounding layers. The phase speed of the cells also increases towards 1 as a result of this.

5.2. The influence of variations in α and δ

Fig. 6 shows how the neutral curve and the corresponding phase speed of the cells vary for different values of α and δ for large fixed values, $d = 1$ and $\mathrm{Pe} = 1$. Results for $\alpha = 10$ and $\alpha = 0.1$ are displayed here, while the intermediate $\alpha = 1$ case may be found as the $d = 1$ case in Fig. 2, for comparison. There is little variation in the neutral curves as α varies over these two orders of magnitude, but the disturbance phase speed depends strongly on α. When α is large, the bounding surfaces are able to react quickly to the moving cells within the porous layer, which causes the phase speed to be close to 1. But when α is small, and especially when k is also relatively small, then heat penetration into the bounding layers is slow, and this reduces greatly the disturbance phase speed.

An illustration of this is given in Fig. 7 when the wavenumber is given by $k = 2$. The streamlines and isotherms for the case $\alpha = 10$ give no indication that there is a horizontal flow in the porous layer, and therefore we may conclude that the bounding layers are reacting very quickly to the moving cells in the porous layer. When $\alpha = 1$, there is an indication of cellular movement, but this is most pronounced when $\alpha = 0.1$, where the thermal drag caused by the low diffusivity in the bounding layers is clearly evident.

5.3. The influence of variations in Pe.

Fig. 8 illustrates how variations in the Péclet number affects the neutral curves and the associated phase speeds. Here we have plotted values of c/Pe in order to compare different cases easily. The $\mathrm{Pe} = 0$ case actually corresponds to $\mathrm{Pe} = 10^{-4}$ as an approximation to the $\mathrm{Pe} \to 0$ limit.

In all cases one finds that increasing values of the Péclet number causes the system to tend towards the Lapwood-Prats problem where $\mathrm{Ra}_c = 4\pi^2$, $k_c = \pi$ and $c_c = \mathrm{Pe}$. That this should happen may be understood by appealing to the fact that when cells pass a given point on the interface between the porous layer and one of the bounding layers, that point will experience very rapid oscillatory changes in the heat transfer. There will be very little time available for the heat in a hot cell to warm up the bounding layer before a cold cell replaces it. Thus the thermal penetration is small when Pe is large, and the phase speed will be almost the same as the value of Pe.

Some streamlines and isotherms are displayed in Fig. 9 for the cases, $Pe = 0$, 1, 10 and 100. In this Figure we have chosen to use the wavenumber corresponding to the respective critical values. We see that the isotherms in the bounding layers become

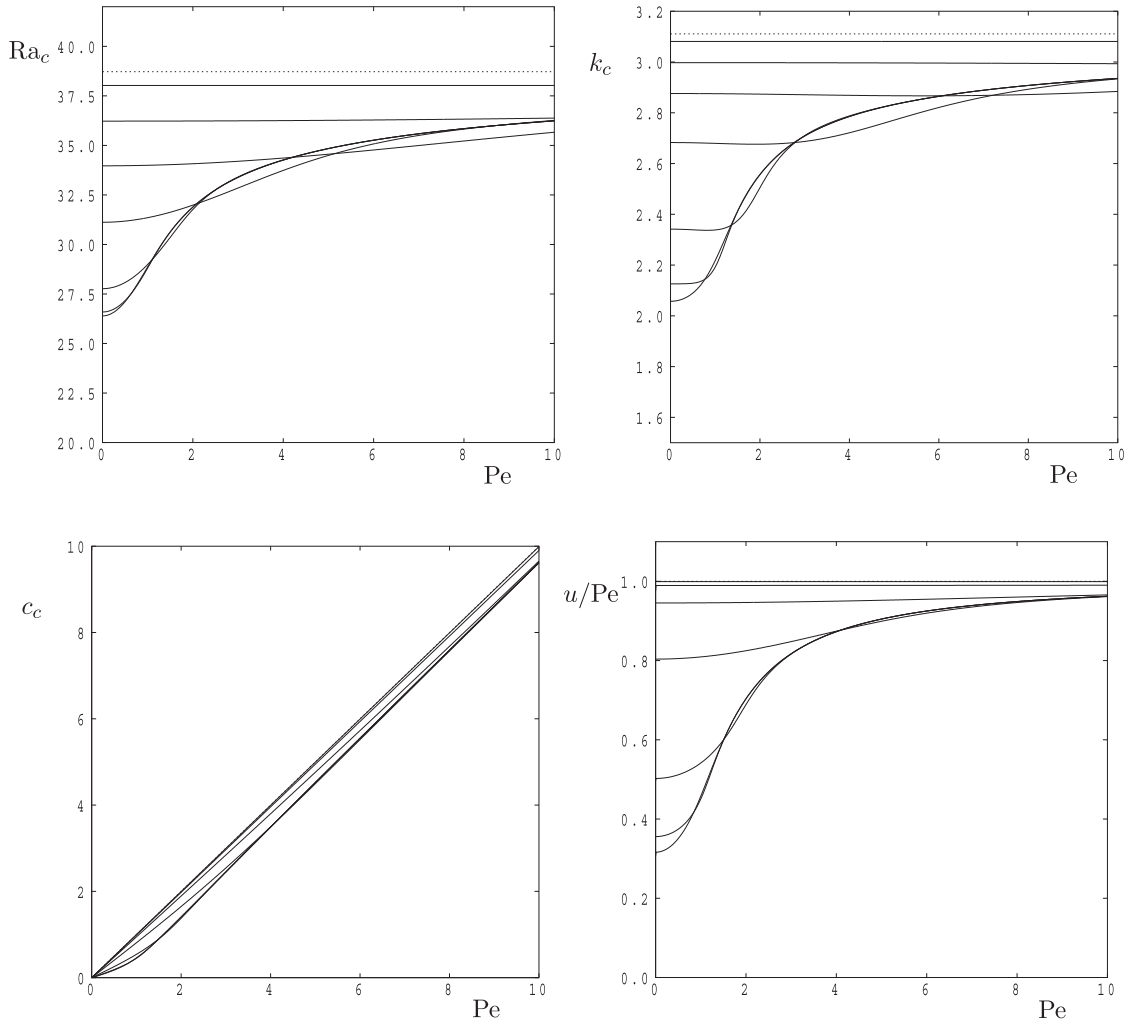

Fig. 12. Critical values for Ra,k,c and c/ Pe as a function of Pe for $d = 1$ and $\alpha = 10$ and for $\delta = 10,1,0.5,0.2,0.1,0.05,0.02$ and 0.01. The dotted line corresponds to $\delta = 0.01$.

increasingly deformed as the Péclet number increases. At the same time the thermal penetration decreases, thereby confirming the above discussion. In addition the critical wavenumber increases towards π, which is equivalent to the disturbance wavelength decreasing towards 2. In the most extreme case, for which Pe = 100, the presence of the thermal disturbance in the bounding layers is shown only by the zero isotherms. These isotherms tend towards the horizontal as Pe increases still further.

5.4. Variation of critical values

We now summarise much of the above and many more cases in Figs. 10–12.

Fig. 10 shows how Ra$_c$,k_c and c_c vary with δ for selected values of d while Pe = α = 1. Both the critical Rayleigh and wave numbers increase as d increases but decrease as δ increases. There is a very distinct value of δ beyond which these critical values do not change and this is because the width of the bounding plates is greater than the thickness of the disturbance field. As the bounding plates decrease in thickness (decreasing δ) the composite layer eventually returns to one which is identical to the single-layer Darcy–Bénard problem. However, the critical phase velocity has a more complicated dependence on d. When d takes very large or very small values either the bounding surfaces resemble very closely the classical Darcy–Bénard problem and are essentially at constant temperature, or else no heat passes into the bounding layers, thereby mimicking the constant-heat-flux form of the Darcy–Bénard problem. In both cases the bounding surfaces play a minimal role and the phase speed of disturbances is approximately the same as the Péclet number. At intermediate values of d, there is a thermal interaction between the porous and the bounding layers and therefore the phase speed decreases.

Variations of the critical values with d for chosen values of δ are displayed in Fig. 11. With regard to Ra$_c$ and k_c, we see the full transition between the constant heat flux (Ra$_c$ = 12 and k_c = 0) and the constant temperature (Ra$_c = 4\pi^2$ and k_c = 12) versions of the Darcy–Bénard problem as d increases. Although we do not show it here, for the sake of brevity, the numerical data suggest strongly that there is a form of similarity solution when $d \ll 1$, namely that Ra$_c$ and k_c each collapse onto one curve when plotted against d/δ. Decreasing values of d and δ correspond respectively to the constant heat flux and the constant temperature single layer models, and therefore the transition between the two depends in a fairly simple way on the relative sizes of d and δ.

Fig. 12 shows the effects of increasing values of Pe on the critical parameters. As discussed above in connection with Fig. 9, an increasing value of Pe causes a return to the Prats case because the cells are moving too quickly to transfer heat into or from the bounding layers. Thus Ra$_c \to 4\pi^2$, $k_c \to \pi$ and c_c/Pe $\to 1$ as Pe $\to \infty$.

5.5. Unusually-shaped neutral curves

We complete our survey of the dependence of the onset criterion on its four governing parameters by exploring one part of

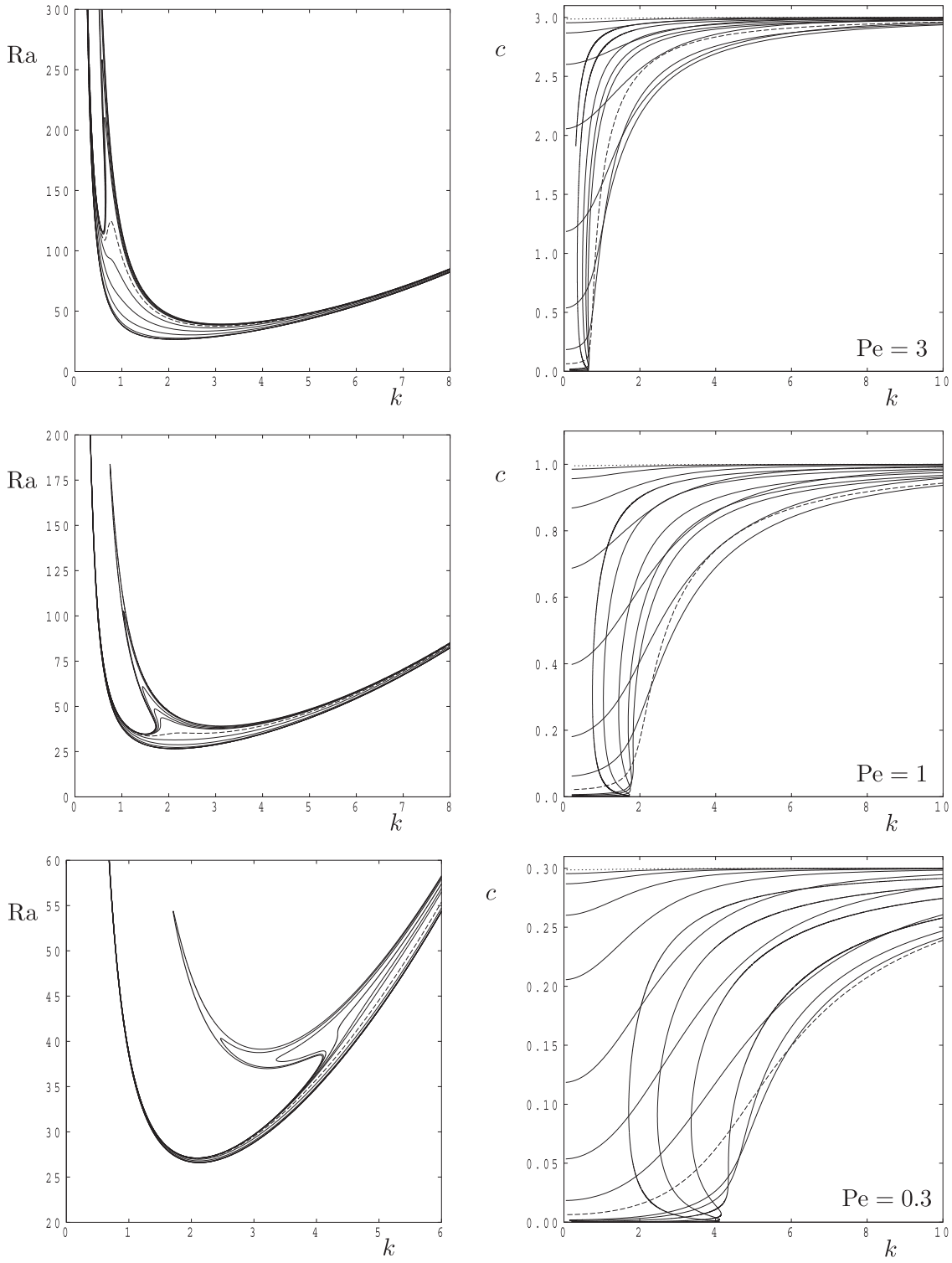

Fig. 13. Neutral curves (left) and the corresponding values of the wavespeed, c, (right) for $d = 1$ and Pe = 1 for the stated values of α. The following values of α were used: α = 100,30,10,3,1,0.3,0.1, 0.03,0.01,0.003 and 0.001. For the case, Pe = 0.3, the value $\alpha = 0.0003$ was also used. The dotted line corresponds to $\alpha = 100$ and the dashed line to $\alpha = 0.01$.

the parameter space where the neutral curves no longer have the standard unimodal shape. As mentioned earlier in the Introduction section, multimodal curves are well-known and often arise in layered systems, such as those studied by Rees and Riley [16] and Proctor and Jones [21]. For the present system we also obtain multimodal curves, but these are not always a single-valued function of the wavenumber. We show three different cases in Fig. 13, and there correspond to different values of the Péclet number, and each subfigure shows neutral curves for a variety of values of α where, in every case, we have $d = \delta = 1$.

When Pe = 3 the left hand branch of the neutral curve first develops a kink as α decreases which then evolves into a curve with two minima. The right hand minimum always remains the one with the lower value of Ra. At still smaller values of α the spike

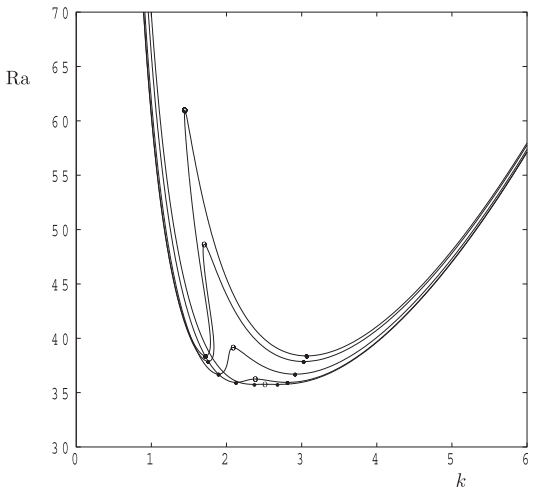

Fig. 14. Neutral curves displaying two minima for the case $d = 1$ and Pe = 1. From the lowest to the uppermost, the curves correspond to $\alpha = 128.75$ ($\delta = 0.231589$), $\alpha = 135$ ($\delta = 0.270102$), $\alpha = 200$ ($\delta = 0.323819$), $\alpha = 500$ ($\delta = 0.346877$) and $\alpha = 1000$ ($\delta = 0.348371$). The bullet symbols denote local minima while the empty circles are local maxima.

in the neutral curve bends to the left, although this is difficult to see directly here: its presence is clear in the numerical data but it may also be inferred by the behaviour of c_c. The Pe = 1 case displays the same behaviour but the left-leaning spike appears at a much larger value of k. The presence of the spike is somewhat misleading since c varies as one traverses the neutral curve. A three-dimensional plot of Ra where k and c are both horizontal coordinates would find the curve travelling in the c-direction at the tip of the spike.

When Pe = 0.3 the overall evolution of the neutral curve is slightly different as α decreases. Instead of first developing two minima, the curve now first becomes multivalued prior to creating a new local maximum and minimum. We see that when $\alpha = 0.0003$ the neutral curve has now developed three minima and two maxima.

By continuity this behaviour must persist in a region of parameter space close to $d = \delta = 1$, although we have not investigated the range of existence of these exotically-shaped curves.

Finally, in Fig. 14, we display some cases where the neutral curves have two minima corresponding to the same Rayleigh number, and allow these minima and the intermediate maximum to merge together. We have taken the values Pe = $d = 1$ for this one illustration. The lowest curve corresponds to a parameter set which is very close to that corresponding to the quartic point, which we estimate as being at $\alpha = 128.64$ and $\delta = 0.2303$ and where $Ra_c = 35.7544$ and $k_c = 2.516$. Other quartic points will exist as either or both of Pe and d are varied.

6. Conclusions

In this paper we have sought to present concisely as much information as we can on the stability characteristics of a porous layer heated from below which is bounded both above and below by conducting impermable layers and where there is an overall background flow along the layer which is driven by an external pressure gradient. The behaviour of the resulting neutral curves cannot always be predicted by means of a simple "addition" of the known effects of conducting bounding layers (viz. a smooth variation between the properties of constant temperature surfaces and constant heat flux surfaces) and of a background flow (viz. a movement of the cells along the layer whwere the phase velocity is identical to that of the background flow). While it is clear that, when Pe takes small values then the stability characteristics are close to that for a zero-Pe layer with conducting bounding layers, and when Pe takes sufficiently large values then we have essentially the situation described by Prats [19] and which is independent of the bounding layers, the transition between these two extremes is not straightforward in all cases. We have found that it is possible for the neutral stability curve to have more than one minimum. But in general the presence of the bounding layers serves to reduce the phase speed of the convection cells relative to that found by Prats [19].

References

[1] C.W. Horton, F.T. Rogers, Convection currents in a porous medium, J. Appl. Phys 16 (1945) 367–370.
[2] E.R. Lapwood, Convection of a fluid in a porous medium, Proc. Cambridge Philos. Soc 44 (1948) 508–521.
[3] D.A.S. Rees, D.S. Riley, The effects of boundary imperfections on convection in a saturated porous layer: non-resonant wavelength excitation, Proc. R. Soc. London A421 (1989) 303–339.
[4] D.A.S. Rees, D.S. Riley, The effects of boundary imperfections on convection in a saturated porous layer: near-resonant wavelength excitation, J. Fluid Mech. 199 (1989) 133–154.
[5] D.A.S. Rees, Stability analysis of Darcy–Bénard convection, Lecture Notes for the Summer School on Porous Medium Flows, Neptun, Constanţa, Romania (25-29 June 2001).
[6] D.A. Nield, Onset of thermohaline convection in a porous medium, Water Resour. Res. 11 (1968) 553–560.
[7] D.A.S. Rees, A. Mojtabi, The effect of conducting boundaries on weakly nonlinear Darcy–Bénard convection, Transp. Porous Media 88 (2011) 45–63.
[8] D.A.S. Rees, The stability of Darcy–Bénard convection, in: K. Vafai (Ed.), Handbook of Porous Media, Marcel Dekker, 2000, pp. 521–558.
[9] P.A. Tyvand, Onset of Rayleigh–Bénard convection in porous bodies, in: D.B. Ingham, I. Pop (Eds.), Transport Phenomena in Porous Media II, Elsevier, New York, 2002, pp. 82–112.
[10] D.A.S. Rees, A. Selim, J.P. Ennis-King, The instability of unsteady boundary layers in porous media, in: P. Vadász (Ed.), Emerging Topics in Heat and Mass Transfer in Porous Media, Springer, 2008, pp. 85–110.
[11] T. Nguyen-Quang, F. Guichard, T.H. Nguyen, Spatial pattern formation of motile microorganisms: From gravititactic bioconvection to protozoan culture dynamics, in: K. Vafai (Ed.), Porous Media: Applications in Biological Systems and Technology, CRC Press, 2010, pp. 535–567.
[12] I. Pop, D.B. Ingham, Convective Heat Transfer: Mathematical and Computational Modeling of Viscous Fluids and Porous Media, Pergamon, Oxford, 2001.
[13] D.A. Nield, A. Bejan, Convection in Porous Media, third ed., Springer, New York, 2006.
[14] R. Rana, R.N. Horne, P. Cheng, Natural convection in a multi-layered geothermal reservoir, A.S.M.E.C: J. Heat Transfer 101 (1979) 411–416.
[15] R. McKibbin, M.J. O'Sullivan, Onset of convection in a layered porous medium heated from below, J. Fluid Mech. 96 (1980) 375–393.
[16] D.A.S. Rees, D.S. Riley, The three-dimensional stability of finite-amplitude convection in a layered porous medium heated from below, J. Fluid Mech. 211 (1990) 437–461.
[17] A. Mojtabi, D.A.S. Rees, The effect of conducting bounding plates on the onset of Horton–Rogers–Lapwood convection, Int. J. Heat Mass Transfer 54 (1–3) (2011) 293–301.
[18] N. Riahi, Nonlinear convection in a porous layer with finite conducting boundaries, J. Fluid Mech. 129 (1983) 153–171.
[19] M. Prats, The effect of horizontal fluid motion on thermally induced convection currents in porous mediums, J. Geophys. Res. 71 (1967) 4835–4838.
[20] D.A.S. Rees, G. Genç, The onset of convection in porous layers with multiple horizontal partitions, Int. J. Heat and Mass Transfer 54 (2011) 3081–3089.
[21] M.R.E. Proctor, C.A. Jones, The interaction of two spatially resonant patterns in thermal convection. Part 1: Exact 1:2 resonance, J. Fluid Mech. 188 (1988) 301–355.